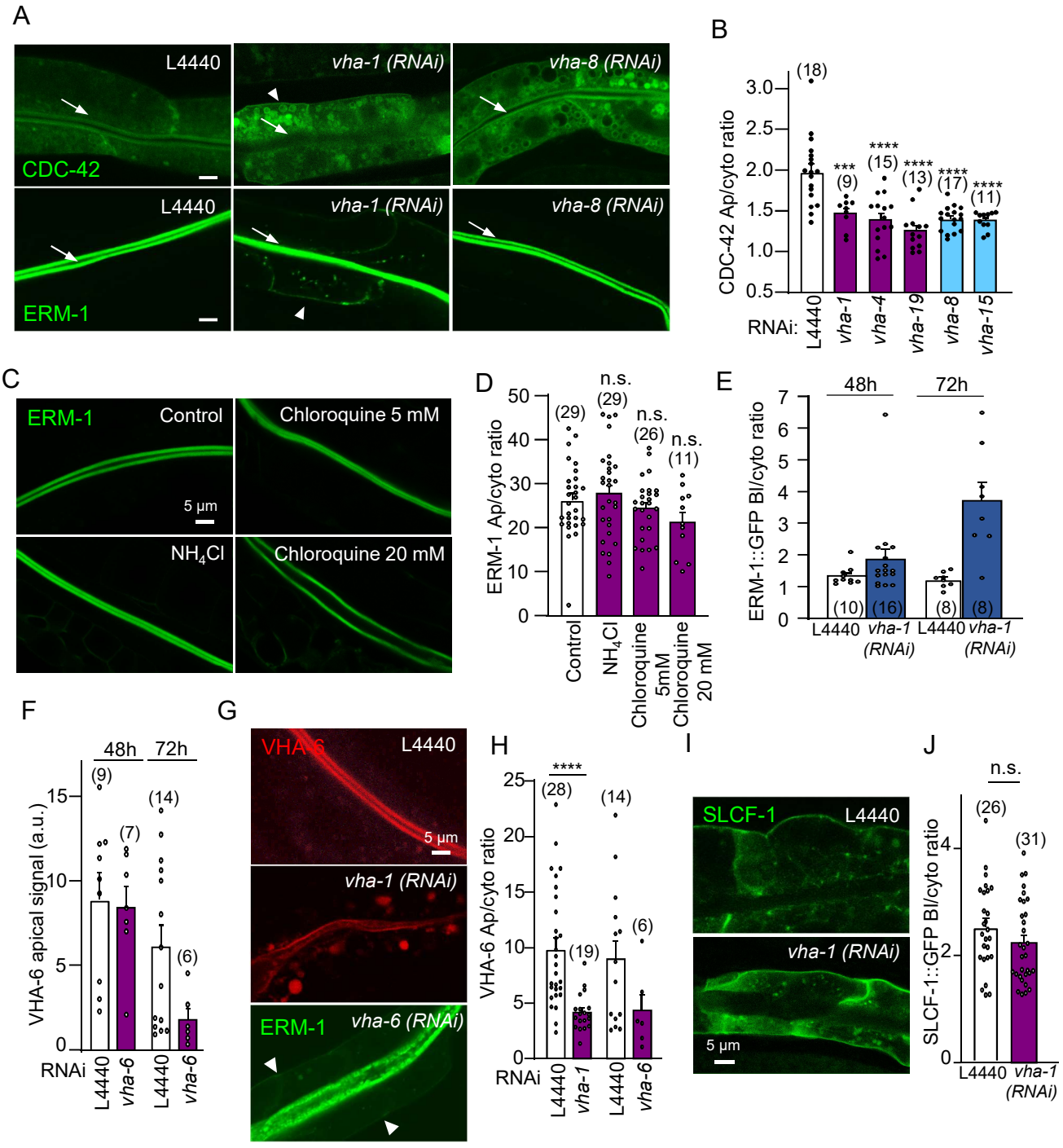

Fig. S1. V0-ATPase silencing affects the polarized localization of polarity modules and brush border components.

(A) Polarity screen results. GFP::CDC-42 (upper panels) and ERM-1::GFP (lower panels) expressing strains were silenced for control (L4440), V0/*vha-1* or V1/*vha-8* specific RNAi during 72h and imaged. Note the basolateral accumulation of both markers upon V0/*vha-1(RNAi)*.

(B) Confirmation of the screen. CDC-42::GFP apical/cytoplasmic ratio was quantified upon silencing of the indicated V-ATPase subunits (n=1).

(C-D) Alkalinization of *C. elegans* intestine does not significantly affect ERM-1 polarized localization. Worms expressing ERM-1::mNG were treated during 24h with M9 alone (control) or supplemented with NH_4Cl (20mM) or Chloroquine (5-20mM) and imaged. (C) shows representative experiments. (D) shows the quantification of ERM-1::mNG apical/cytoplasmic ratio (n=2).

(E) Time-dependent measurement of V0/*vha-1* effect on ERM-1 basolateral mislocalization. ERM-1::GFP expressing worms were silenced for V0/*vha-1* during 48 or 72h, imaged and ERM-1 basolateral/cytoplasmic ratio was quantified (n=1).

(F-H) Effect of 48-72h V0/*vha-1/6(RNAi)* on the expression of the V0-ATPase subunit VHA-6::mCh and the localization of ERM-1::GFP. (F) shows the quantification of VHA-6::mCh apical signal after 48h or 72h *vha-6(RNAi)* (n=1). (H) shows the quantification of VHA-6::mCh apical/cytoplasmic ratio in worms silenced for control (L4440), *vha-1* (n=3) or *vha-6* (n=1). Arrowheads in (G) show the basolateral mislocalization of ERM-1 upon *vha-6(RNAi)*.

(I-J) Effect of 72h V0- or V1-ATPase silencing on the basolateral/cytoplasmic ratio of SLCF-1 (n=3). (H) shows a representative experiment. The histogram shows the mean ± SEM, dots represent individual worms and the total number of worms is indicated in brackets. n.s. non-significant, ***p<0.001, ****p<0.0001. Arrows and arrowheads show the apical and basolateral PM, respectively. In all micrographs, worms are at the L4/young adult developmental stage.

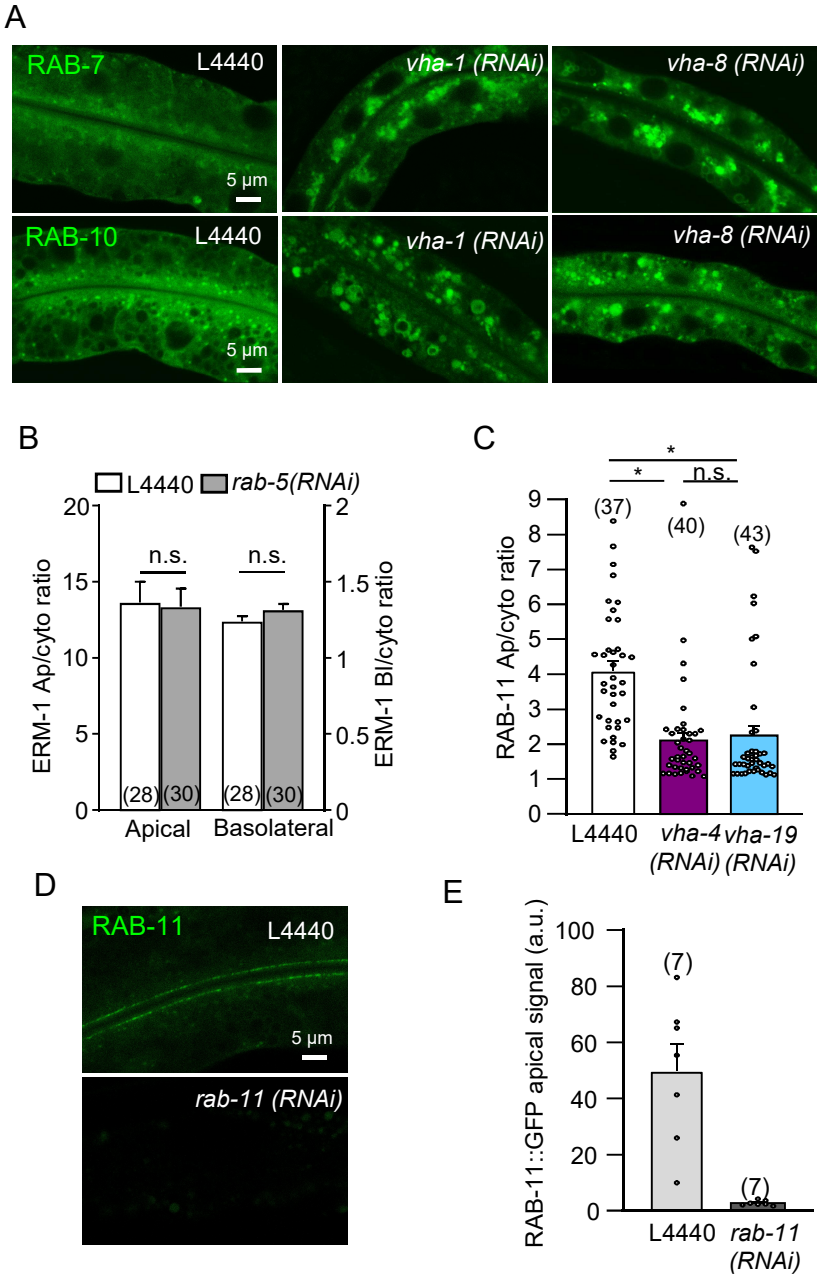

Fig. S2. V0-ATPase polarity maintenance pathway.

(A) Both V0/*vha-1* and V1/*vha-8(RNAi)* (72h) induce an accumulation of GFP::RAB-7 and GFP::RAB-10 in large cytoplasmic structures. Image shown is representative of 52-66 RAB-7::GFP and 38-58 RAB-10::GFP expressing worms observed for each condition, out of 3-5 independent experiments.

(B) *rab-5(RNAi)* does not affect the polarity of ERM-1. *rab-5* was silenced by RNAi during 72h in a strain expressing ERM-1::GFP, imaged and the apical/cytoplasmic (left) and basolateral/cytoplasmic (right) ratios of ERM-1 were quantified.

(C) Knockdown of the V0-ATPase subunits *vha-4* and *vha-19* induces a loss of RAB-11^{+} endosomes. Histogram represents the quantification of the apical/cytoplasmic ratio of RAB-11::GFP. Mann-Whitney U-test.

(D-E) *rab-11(RNAi)* decreases RAB-11:GFP expression. (G) shows the quantification of RAB-11::GFP apical/cytoplasmic ratio.

Histograms are mean ± SEM on each panel, dots represent individual worms and the total number of worms from 2 (B-C) or 1 (E) independent experiment(s) is indicated in brackets. n.s. non-significant, *$p<0.05$. In all micrographs, worms are at the L4/young adult developmental stage.

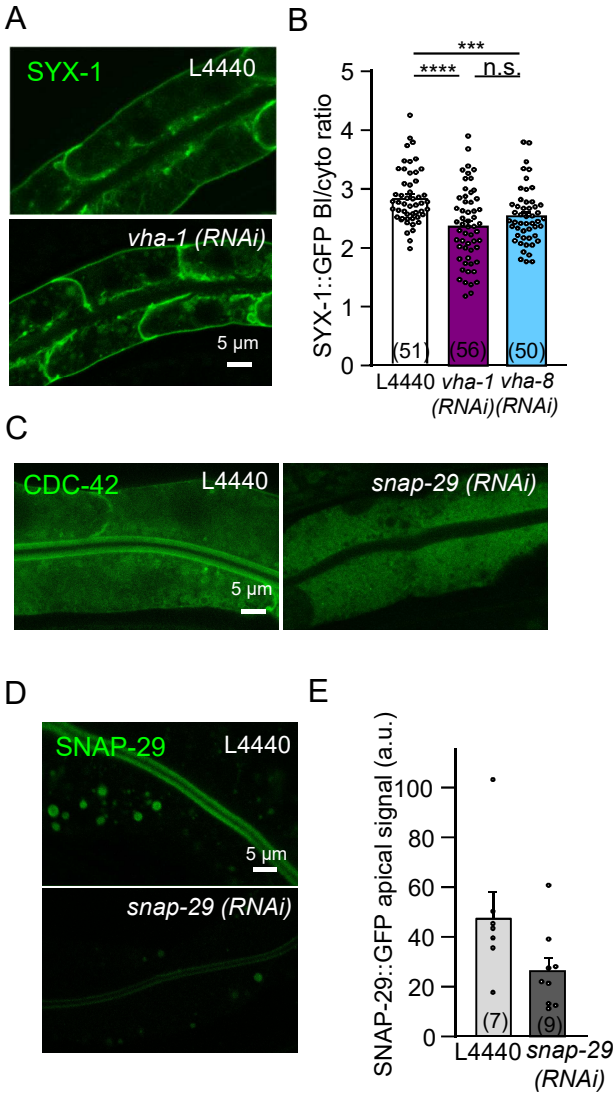

Fig. S3. V0-ATPase polarity maintenance pathway.

(A-B) Effect of 72h V0- or V1-ATPase silencing on the basolateral/cytoplasmic ratio of SYX-1/SYN-1. Left panel shows a representative experiment.

(C-E) *snap-29(RNAi)* decreases CDC-42::GFP apical localization and SNAP-29::GFP expression. (E) shows the apical/cytoplasmic ratio of SNAP-29::GFP.

Histograms are mean ± SEM on each panel, dots represent individual worms and the total number of worms from 3 (B) or 1 (E) experiment(s) is indicated in brackets. n.s. non-significant, *p<0.05, ***p<0.001, ****p<0.0001. In all micrographs, worms are at the L4/young adult developmental stage.

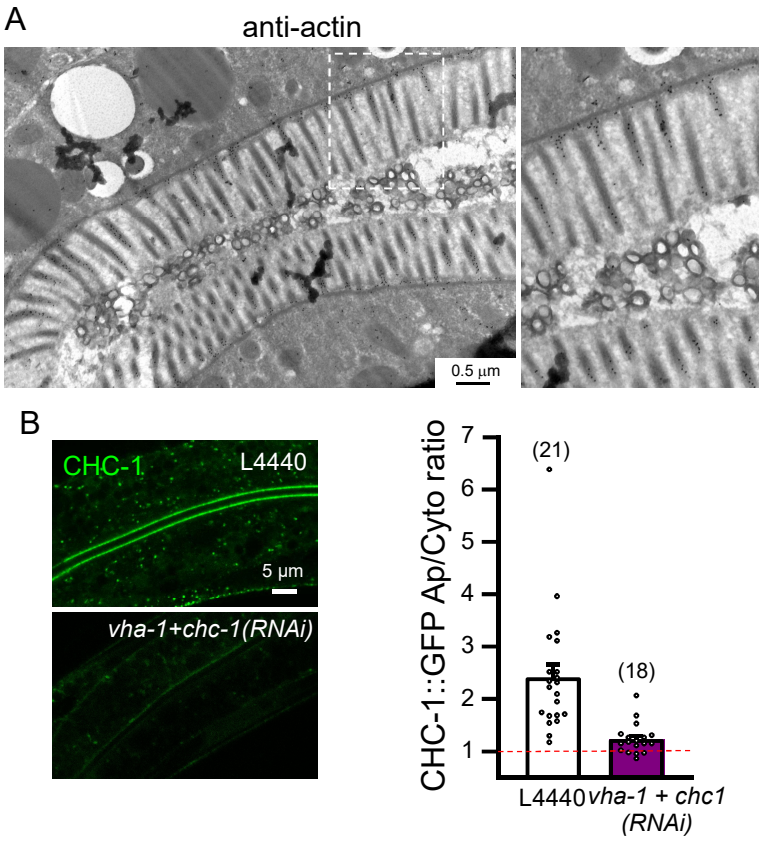

Fig. S4. Controls of ACT-5::mCh staining and *chc-1* knockdown.

(A) Fast-hybrid Tokuyasu-based immuno-EM on young adults using anti-actin antibody and protein A gold allows to visualize actin at both the microvilli and the terminal web level. Right micrograph shows an higher magnification of the selected area.

(B) Control of *vha-1*/*chc-1* genetic interaction. To evaluate *chc-1* silencing in genetic interaction experiments, CHC-1::GFP expressing worms were silenced for control (L4440) or equal amount of *vha-1* and *chc-1(RNAi)* in parallel of an ERM-1::GFP experiment (Fig. 5C) and imaged. Right panel shows the quantification of CHC-1::GFP apical/cytoplasmic ratio (n=1). Dotted line indicates a ratio of 1, which corresponds to an absence of apical enrichment. Histogram is mean ± SEM, dots represent individual worms and the total number of worms is indicated in brackets. In micrographs, worms are at the L4/young adult developmental stage.

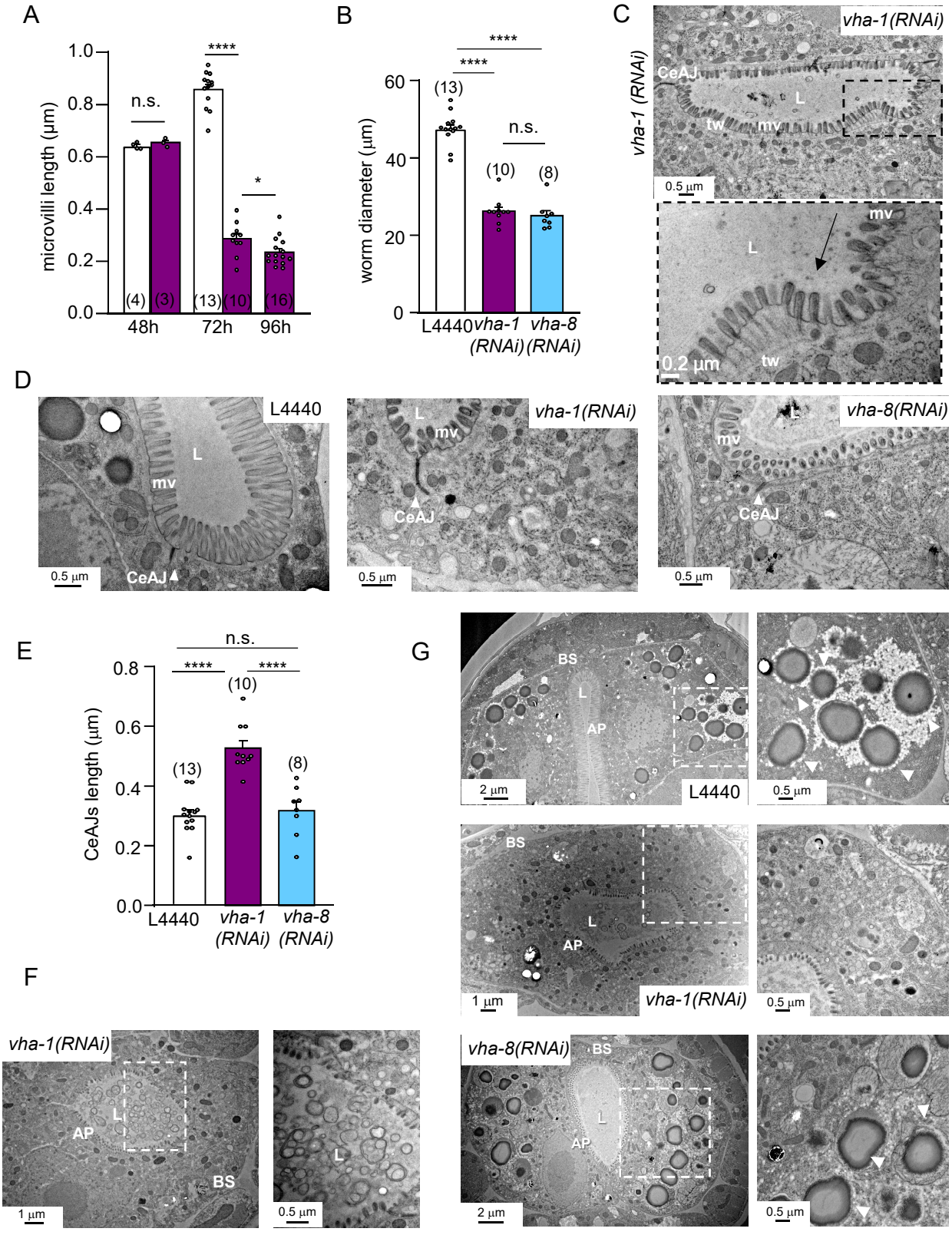

Fig. S5. Ultrastructural analysis of V0-ATPase silencing associated defects.

(A) V0/*vha-1(RNAi)* structural defects appear after 72h silencing. Histogram shows the measurement of microvilli length from TEM images (n=5 microvilli measured/worm).

(B) V0- or V1-ATPase subunits silencing affects *C. elegans* development. Histogram shows the measurement of the worms' diameter from TEM images.

(C-E) V0/*vha-1* silencing often induced a detachment of the PM from the terminal web (C) as well as (D-E) increased the length of cell junctions (CeAJ). (E) shows the measurement of the electron-dense cell-cell junction length on TEM pictures.

(F) V0/*vha-1* depleted worms accumulate cell and/or bacterial debris in the intestinal lumen.

(G) V0/*vha-1* depleted N2 worms, contrary to control or V1/*vha-8*-depleted worms, are devoid of yolk storage granules (arrows). L, lumen; mv, microvilli; tw, terminal web; AP, apical PM; BS, basal PM; CeAJ, *C. elegans* adherens junctions.

In micrographs, worms are at the L4/young adult (72h RNAi) or adult (96h RNAi) developmental stage. Histograms show the mean ± SEM, dots represent individual worms and the total number of worms is indicated in brackets. n.s. non-significant, *p<0,05, ****p<0,0001.

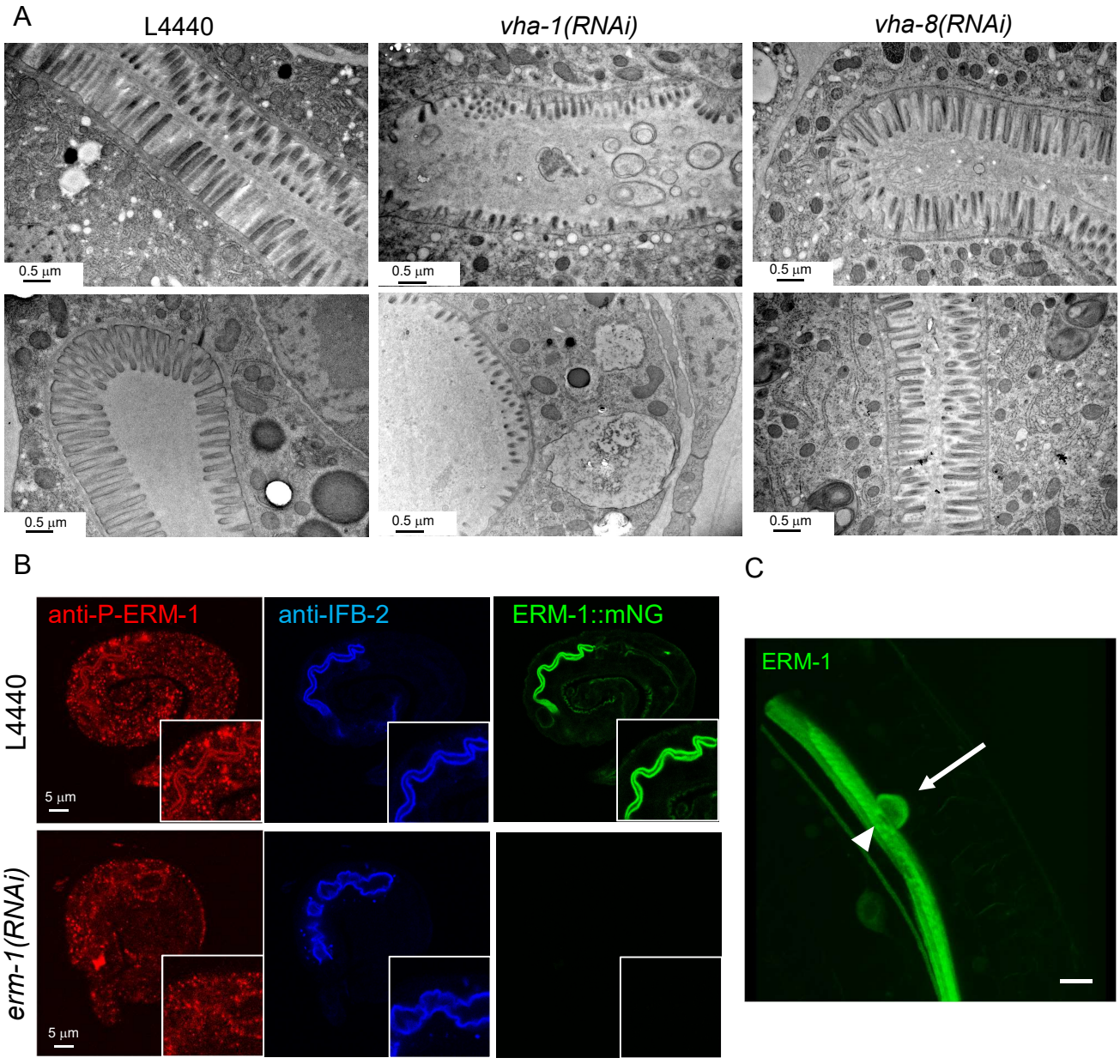

Fig S6. Terminal web integrity upon V-ATPase silencing, P-ERM-1 antibody validation and MVIs onset by internalization of the apical PM.

(A) The terminal web is preserved upon both V0/*vha-1* and *vha-8(RNAi)* silencing. L4440, *vha-1(RNAi)* or *vha-8(RNAi)* treated L4/young adults worms (72h) were analysed by TEM.

(B) Control of P-ERM-1 antibody. ERM-1::mNG expressing worms were silenced or not (L4440) for *erm-1*. Then, 3-fold stage embryos were fixed and stained for P-ERM-1 (red) or IFB-2 (MH33, blue) and imaged. Inserts are magnified selected areas.

(C) 3D projection of ERM-1::GFP expressing worms silenced for V0/*vha-1* during 72h. The arrow indicates the internalization of the apical PM. Note the large hole induced by the PM invagination (arrowhead). Scale bar: 5 μm.

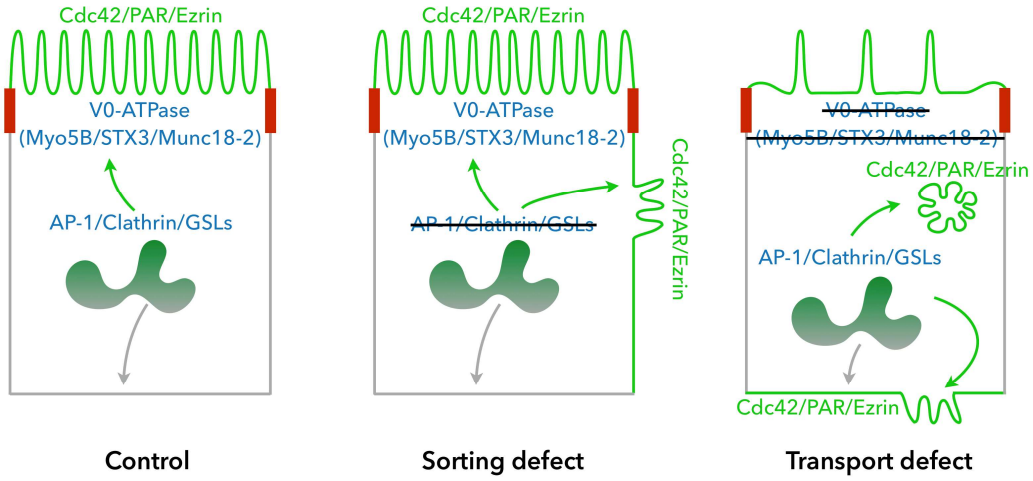

Fig S7. Comparison of polarity maintenance pathways.

In control cells, AP-1, Clathrin and GSLs ensure the correct sorting of polarity and brush border proteins, directly or through adaptor proteins, to the apical PM. PM targeting likely involves RAB-11^{+} apical recycling endosomes, from which polarity/brush border/adaptors-containing vesicles fuse with the PM in a V0-ATPase/Myo5B/STX3/Munc18-2-dependent manner. Upon AP-1 and/or Clathrin and/or GSLs silencing, the early apical sorting step is defective, leading to a polarity inversion that induces the lateral accumulation of apical factors and the formation of lateraly positionned ectopic apical membranes. Upon V0-ATPase or Myo5B/STX3/Munc18-2 silencing, a late apical exocytosis step is defective, which affects only trafficking (i.e. SNAP-29 or STX3) and induces the misrouting of polarity/brush border components to the basolateral PM or in MVIs.

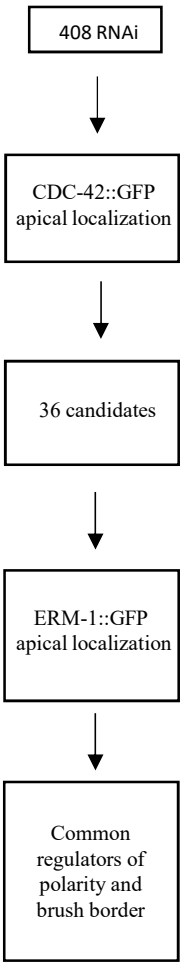

Family	Gene
COPI	*E03H4.8/COP1*
	copb-1/COPI beta
	copz-1/COPI zeta
	copb-2/COPI beta prime
Cytoskeleton	*act-5*
	tba-1
	tba-2
ECM	*noah-1*
ER traffic	*lpin-1*
Vesicle transport	*sam-4*
GSL	*fasn-1*
	pod-2
	sptl-1
Membrane fusion	*nsf-1*
	snap-29
	snap-1
Muscle	*let-805*
	vab-10
	pat-10
NADPH oxidase	*bli-3*
Sorting	*aps-1*
	chc-1
PAR	*cdc-42*
Rabs	*rab-5*
Ribosome	*rpl-36*
V-ATPase	*vha-4*
	unc-32
	vha-1
	vha-19
	vha-17
	vha-15
	vha-20
	vha-10
	vha-8
	vha-12
Others	*Uncharacterized protein family, transmembrane-17*

Table S1. Polarity maintenance screen results. White and blue cases indicate the genes that affect CDC-42 apical localization and basolaterally mislocalize ERM-1, respectively.

Table S2: Comparison of V0/*vha-1* and V1/*vha-8* silencing phenotypes

	L4440	***vha-1(RNAi) (V0)***	***vha-8(RNAi) (V1)***
CDC-42, PAR-6, PKC-3, ERM-1 apical PM	Normal	Down	Down (except ERM-1)
Basolateral PAR-6, PKC-3, ERM-1	No	Yes	No
SNAP-29 cytoplasmic accumulation	No	Yes	No
Mixed organelles	No	Yes	Yes
LMP-1, RAB-7, RAB-10 accumulation	No	Yes	Yes
Autophagy activation	No	+++	+
Accumulation of cytoplasmic lucent vesicles	No	Yes	No
RAB-11 signal	-	Down	Up
Microvillus atrophy	No	Yes	No
MVIs, vacuoles	No	Yes	No

Table S3 : Comparison of MVID and V0-ATPase depletion phenotypes.
Adapted from (49), with minor modifications.

MVID phenotype	Normal intestine	*MYO5B* deficient patients	*STX3* deficient patients	*MUNC18-2* deficient patients (FHL5)	*MUNC18-2* $^{-/-}$ mouse organoids	*vha-1* RNAi *C. elegans*
microvillus atrophy (absent or abnormal microvilli)	no	yes	yes	yes	yes	yes (Fig 4)
microvillus inclusions	no	frequent, observed in 10% of cells	infrequent	infrequent, not fully penetrant	frequent but only after differentiation	infrequent (Fig 5)
basolateral microvilli	no	incomplete penetrance	frequent	frequent	frequent but only after differentiation	probable (Fig 5)
vesicle or tubulo-vesicular structures accumulation	no	Apical vesicles and tubulovesicular; variable electron-dense and translucent	Apical vesicles and tubulovesicular; variable electron-dense and translucent (villus)	electron-dense and translucent apical vesicles	crypt: translucent apical villus: translucent tubulovesicular apical	endosome like vesicles and enlarged vacuolar structures (Fig 2)
RAB-11+ apical recycling endosomes loss	no	yes	yes	yes	yes	yes (Fig 2)
lysosomal abnormalities	no	Enlarged (auto)lysosomes	Enlarged (auto)lysosomes	high number of lysosomes	enlarged lysosomes	enlarged and high number of lysosomes (Fig 2)
STX3 localization	apical membrane	Subapical vesicle and MVIs	reduced/absentprote in level	subapical vesicle and MVIs	diffuse in cytoplasm	UNC-64 (STX3 ortholog) membrane accumulation (Fig 3)
Brush border proteins defects (ERM-1, ACT-5)	strong in brush border	Reduced brush border signal, MVIs positive	presence of dot- and ring-like structures	reduced brush border, MVIs stained; variable penetrance and severity	reduced brush border, cytoplasmic foci and MVIs stained	reduced brush border, presence of MVI structures (Fig 1, 4, 5, 6)

Table S4: *C. elegans* strains used in this study

Strain name	Genotype	Reference
DA2123	*adIs2122 [lgg-1p::GFP::lgg-1 + rol-6(su1006)]*	CGC
FL274	*erm-1(bab59[erm-1::mNG^SEC^3xFlag]) I ; ifb-2(bab142[ifb-2::wSc]) II*	This study
FL316	*dfEx3 [vha-6p::gfp::cdc-42 + rol-6 (su1006)]; unc-119(ed3)III; mcls46 [dlg-1::rfp+unc-119(+)]*	This study
FL368	*bls5[chc-1p::gfp::chc-1 + rol-6(su1006)]; jyls17 [vha-6p::mcherry::act-5, ttx-3p::RFP]*	This study
FL369	*fgEx13[perm-1::erm-1::gfp + rol-6 (su1006)] ; jyIs17 [vha-6p::mcherry::act-5, ttx-3p::RFP]*	This study
FL373	*pkc-3(it309[GFP::pkc-3]) II; erm-1(bab64[erm-1::wrmSc^3xFlag]) I*	This study
FL374	*rnyEx60 [pELA2 (vha-6p:::vha-6::mCherry) + myo-3p::GFP + pCL1 (pha-1+)]; pwIs69 [vha6p::GFP::rab-11 + unc-119(+)]*	This study
FL375	*unc-119(ed3) III; pwIs69[vha6p::GFP::rab-11 + unc-119(+)]; rnyEx60 [pELA2 (vha-6p::vha-6::mCherry) + myo-3p::GFP + pCL1 (pha-1+)]*	This study
FL376	*pwIs50 [lmp-1::GFP + Cbr-unc-119(+)]; erm-1(bab64[erm-1::wrmSc^3xFlag]) I*	This study
FL378	*erm-1(bab59[erm-1::mNG^SEC^3xFlag]) I*	This study
FL379	*erm-1(bab64[erm-1::wrmSc^3xFlag]) I*	This study
FS254	*slcf-1(tm2258); Exfs254[slcf-1::gfp]*	Mouchiroud et al., 2010
GK385	*unc-119(ed3) ; dkIs218[Popt-2-GFP-syn-1 ; Cb.unc-119(+)]*	Sato et al., 2011
GK446	*unc-119(ed3) ; dkIs259[Pact-5-GFP-snap-29 ; Cb.unc-119(+)]*	Sato et al., 2011
KK1228	*pkc-3(it309[GFP::pkc-3]) II*	CGC
KK1248	*par-6(it319[par-6::GFP]) I*	CGC
KWN117	*rnyEx60 [pELA2 (vha-6p:::vha-6::mCherry) + myo-3p::GFP + pCL1 (pha-1+)]*	CGC
KWN246	*pha-1(e2123) III, rnyEx133[opt-2(aa1-412)::GFP) + pha-1(+)]*	CGC
MCP111	*pgp-1(bab111[mNG^3xFlag::pgp-1]) IV*	This study
MCP91	*unc-64(bab91[wrmSc^3xFlag ::unc-64]) III*	This study
RT258	*pwIs50 [lmp-1::GFP + Cbr-unc-119(+)]*	CGC
RT311	*pwIs69 [vha6p::GFP::rab-11 + unc-119(+)]*	CGC
RT327	*pwIs72 [vha-6p::GFP::rab-5 + Cbr-unc-119(+)]*	CGC
RT476	*pwIs170 [vha6p::GFP::rab-7 + Cbr-unc-119(+)]*	CGC
RT525	*pwIs206 [vha6p::GFP::rab-10 + Cbr-unc-119(+)]*	CGC
VJ268	*fgEx12[pact-5::act-5::gfp]*	Zhang et al., 2012
VJ500	*let-767(s2176) dpy-17(e164) unc-32(e189)III; sDp3(III;f); fgEx13[perm-1::erm-1::gfp rol-6(su1006)]*	Zhang et al., 2011

Table S5. List of the targeted genes in the RNAi screen.

Click here to Download Table S5

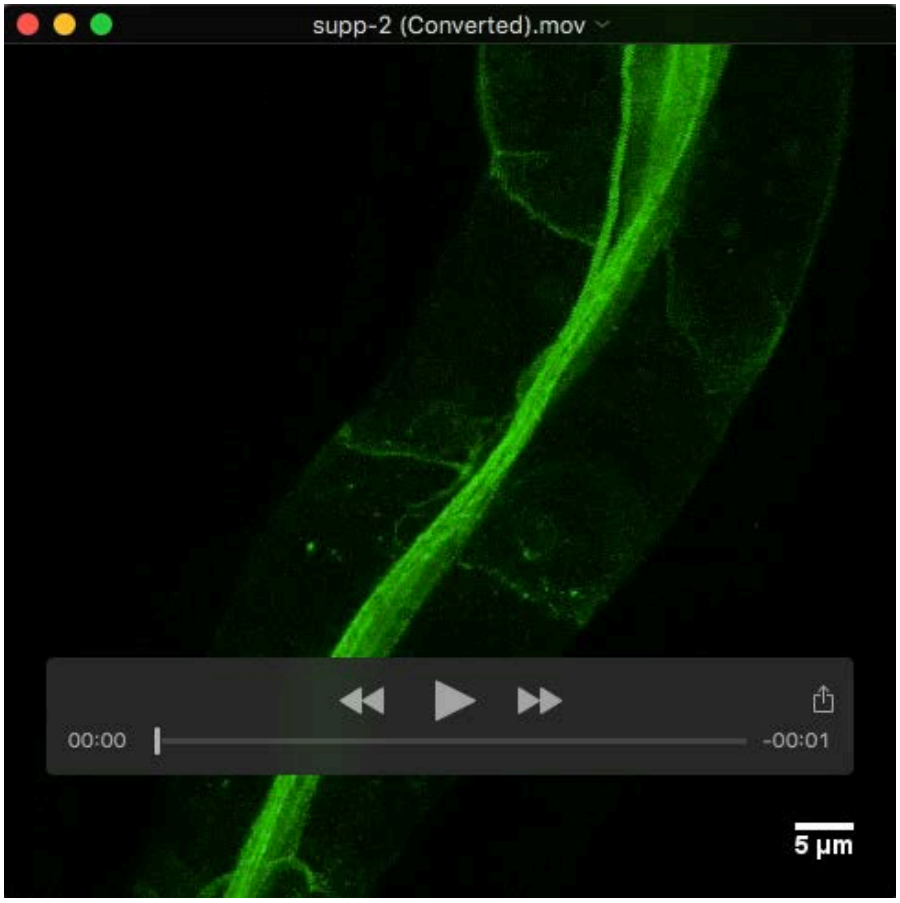

Movie 1. Cytoplasmic nucleation of MVIs. Maximum projection of ERM-1::mNG expressing worms silenced for V0/*vha-1* during 96h. Arrows indicate nucleating MVIs.

Movie 2. Cytoplasmic nucleation of MVIs. Maximum projection of ERM-1::mNG expressing worms silenced for V0/*vha-1* during 96h. Arrowheads and arrows indicate irregular MVIs/vacuoles and cytoplasmic nucleating MVIs, respectively.

Movie 3. MVI formation by internalization of the apical PM. 3D projection of ERM-1::GFP expressing worms silenced for V0/*vha-1* during 72h.

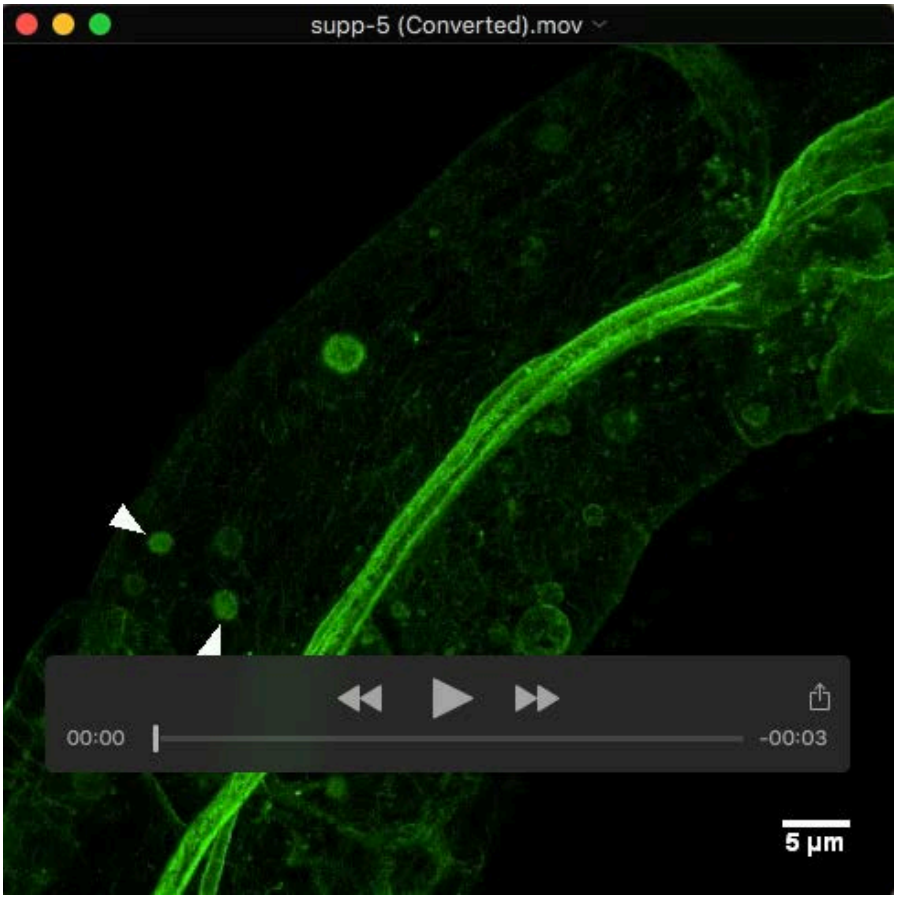

Movie 4. MVI elimination. Maximum projection of ERM-1::mNG expressing worms silenced for V0/*vha-1* during 96h. The arrow indicates the elimination of the MVIs inside the presumptive autophagic ERM-1^{+} membrane. Arrowheads show direct MVI disappearance in the cytoplasm.